ACS Energy LETTERS

http://pubs.acs.org/journal/aelccp

Letter

Mechanistic Insights into Sodium Plating in Hard Carbon Anodes: Electrolyte Design Principles for Practical Medium Voltage Sodium-Ion Full Batteries

Published as part of ACS Energy Letters special issue "The Evolving Landscape of Energy Research: Insights from Leading Researchers".

Yuejing Zeng,[#] Wei Li,[#] Yuan Qin, Yang Yang,* and Jinbao Zhao*

Cite This: https://doi.org/10.1021/acsenergylett.5c04116

Read Online

ACCESS | Metrics & More | Article Recommendations | Supporting Information

ABSTRACT: Hard carbon (HC) is a leading anode for sodium-ion batteries (SIBs), yet its practical application is hindered by Na plating stemming from its multistage Na-storage mechanism, which generates quasi-metallic Na clusters near the deposition potential, triggering uncontrolled metal deposition. Despite numerous advances in electrolyte design that improve cycling stability, the electrolyte dependence of Na plating is poorly understood. Herein, the Na plating behavior of HC in practical pouch-type full cells is systematically investigated, establishing electrolyte design principles that highlight the necessity of addressing Na plating/stripping reversibility alongside Na^+ insertion/extraction. Na plating is found to be intrinsic and unavoidable under realistic operating conditions, including fast charging, prolonged cycling, and low-temperature cycling. Comparative analysis of ester-based (EC/DEC) and ether-based (G2) electrolytes reveals that the G2 electrolyte enables highly reversible Na plating/stripping, attributed to its lower desolvation barrier, faster interfacial kinetics, and the formation of an inorganic-rich solid electrolyte interphase (SEI). These findings underscore the importance of jointly enhancing the Na plating reversibility and SEI robustness for next-generation HC-based SIBs. Notably, ether-based formulations are validated as suitable for coupling low-voltage cathode systems, mitigating N/P ratio constraints, and unlocking higher energy densities.

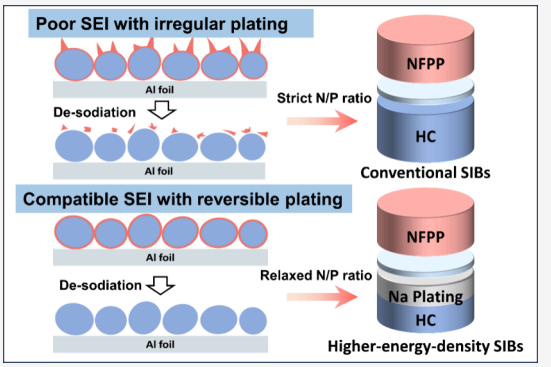

The accelerating transition to renewable energy has intensified the need for cost-effective and durable energy storage systems. Sodium-ion batteries (SIBs), benefiting from earth-abundant of sodium resources, low cost, and chemical similarity to lithium-ion batteries (LIBs), have emerged as a compelling candidate for large-scale deployment.[1−4] However, their practical viability is critically dependent on the performance of anode materials, which fundamentally governs cycling stability and safety. Among the available options, Hard carbon (HC) stands out for its high specific capacity, low cost and good cycling stability, making it the most promising anode material for commercial SIBs.[5−7]

Despite its promise, the practical performance of HC in a full cell often lags behind that observed in a half-cell test, with Na plating identified as a key challenge. This issue originates from the intrinsic multistage Na storage mechanism of HC, which involves adsorption, interlayer insertion and pore filling accompanied by the formation of quasi-metallic Na clusters, a mechanism that is currently considered one of the mainstream interpretations.[6,8] The nanoscale quasi-metallic Na clusters generated at this regime are highly reactive and readily reduce electrolyte species to form a heterogeneous and unstable solid electrolyte interphase (SEI) that continuously consumes active Na and increases interfacial resistance. Moreover, at deep discharge (typically below 0.05 V vs Na/Na^+), the voltage plateau is already near the deposition potential of metallic Na (Scheme 1a),[9−11] rendering Na plating highly susceptible to occur even under standard operating conditions.[12,13] By contrast, graphite in LIBs operates relatively higher than the Li deposition potential (about 0.1 V vs Li/Li^+) and forms the stable LiC_6 intercalation compound (Scheme 1b), making Li plating relatively controllable through rational design.[14,15] Therefore, the inherent Na storage mechanism of HC implies

Received: December 11, 2025
Revised: January 12, 2026
Accepted: January 26, 2026

Scheme 1. (a) Schematic Illustration of the Na-Storage Mechanism in HC at Different Stages; (b) Schematic Diagram of the Lithiation Process in Graphite

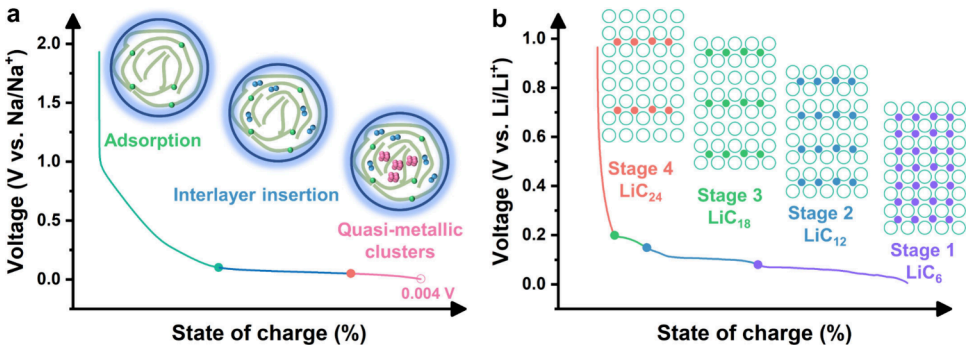

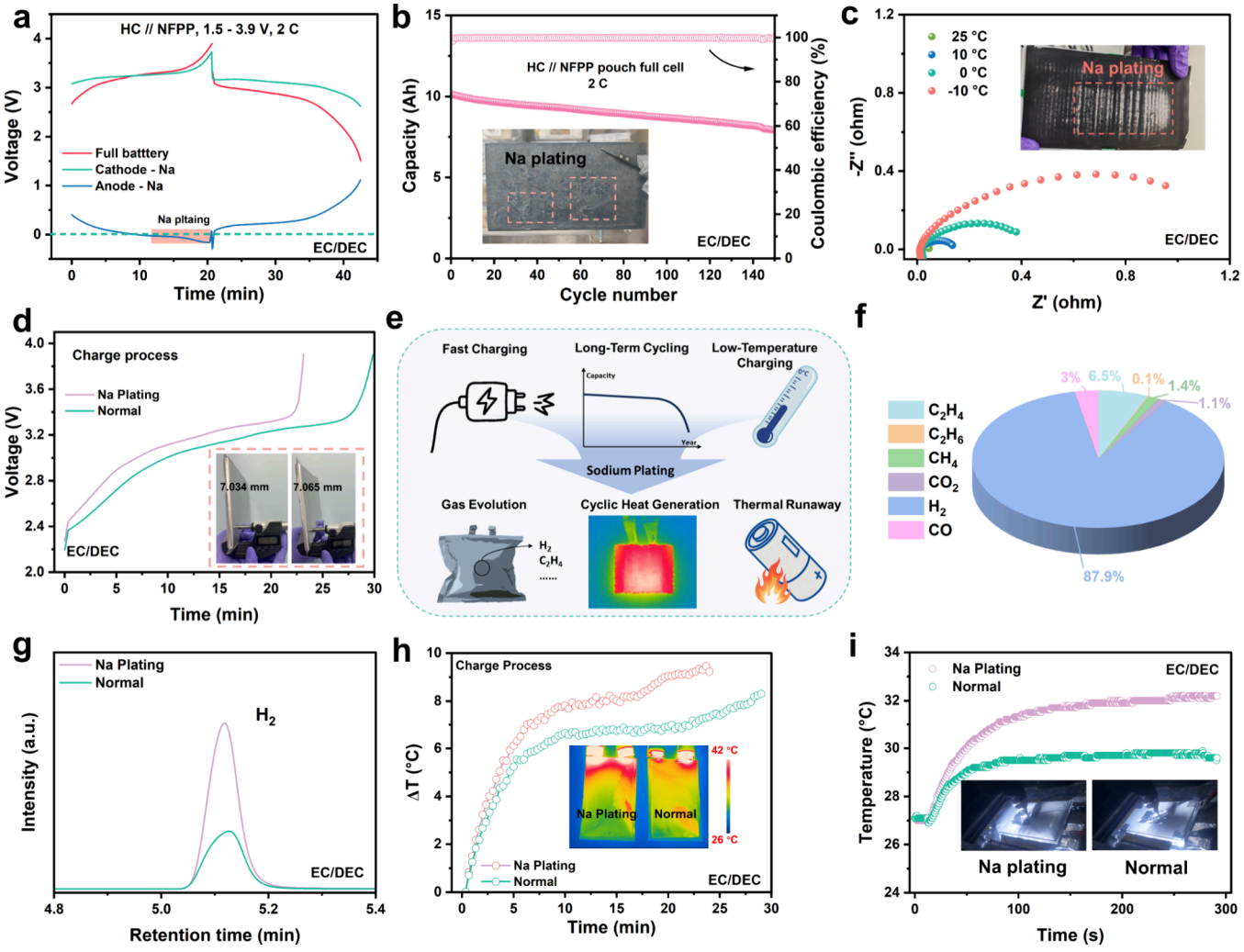

Figure 1. (a) Voltage profiles of the three-electrode HC//NFPP cell at 2 C with Na metal reference electrode. (b) Cycling performance of pouch full cell HC//NFPP and electrode image after cycling, indicating Na plating. (c) The EIS spectra of HC//NFPP pouch cell at different temperatures, with electrode photo after cycling at 0 °C. (d) Voltage curves of SIB pouch cell under different operational states with optical photographs. (e) Schematic illustrating possible Na plating scenarios and associated hazards. (f) Gas composition of SIB pouch cell through GC measurements. (g) H_2 evolution measured by titration gas chromatography on normal electrode and electrode after cycling. (h) Temperature profiles of SIB pouch cells during charging with representative FLIR images. (i) Temperature profiles of SIB pouch cells under nail penetration test.

that Na deposition may be unavoidable, constituting a critical bottleneck for SIB safety and longevity.[16,17]

Efforts to mitigate Na plating have primarily focused on anode structural optimization and electrolyte formulation. Among these, electrolyte design plays a pivotal role, as it not only governs Na^+ transport but also defines the interfacial properties and SEI stability. Consequently, electrolyte that promote robust SEI formation and accelerate Na^+ desolvation have been identified as one of the most effective strategies to suppress plating.[18−21] For instance, Liang et al.[22] demonstrated

https://doi.org/10.1021/acsenergylett.5c04116
ACS Energy Lett. XXXX, XXX, XXX−XXX

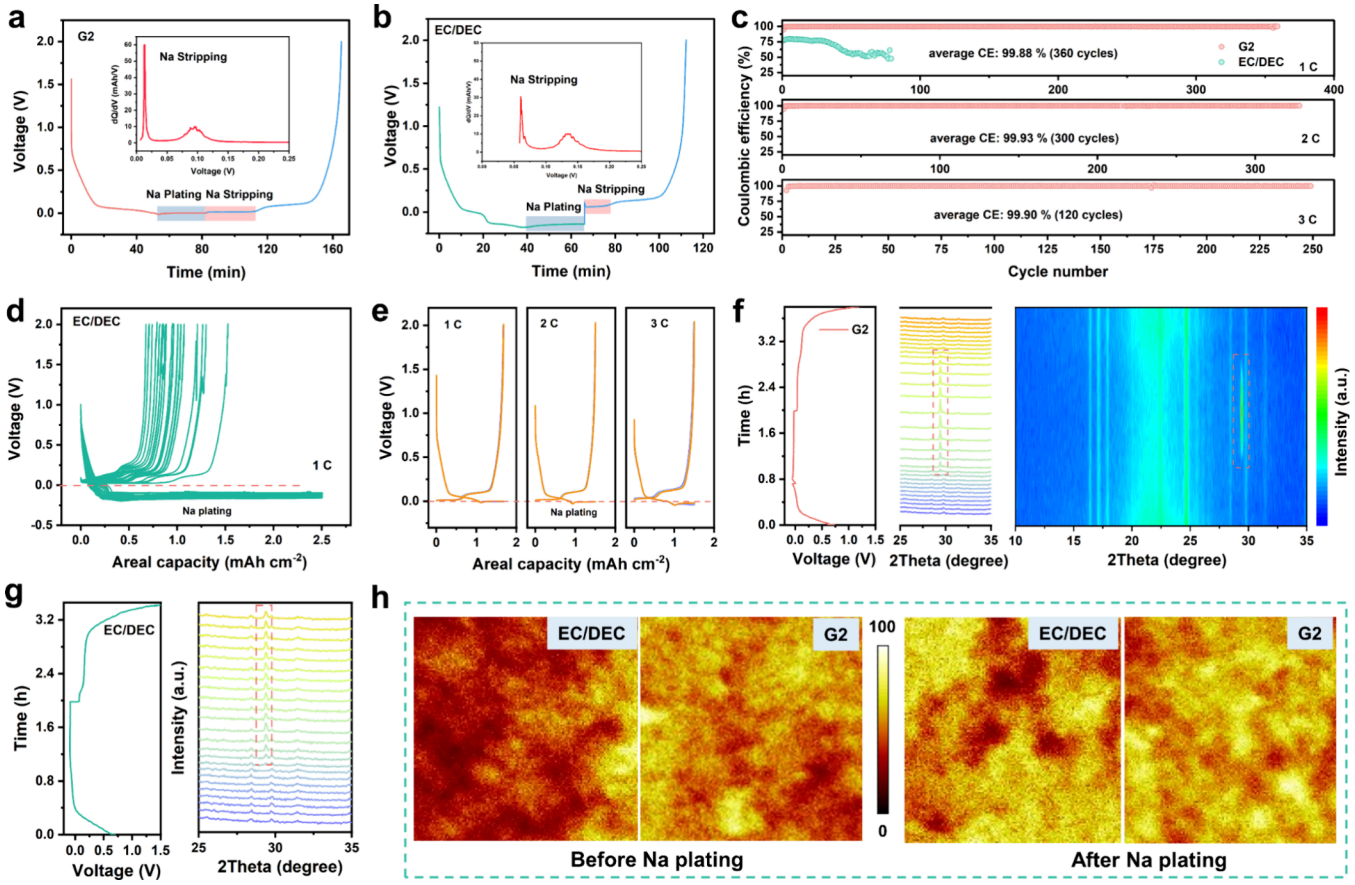

Figure 2. Voltage−time curves of cells using G2 (a) and EC/DEC (b) electrolytes. (c) CE of Na//HC half cells with G2 and EC/DEC electrolytes at 1, 2, and 3 C. (d) Capacity-voltage curves of cell using EC/DEC electrolyte at 1 C. (e) Capacity-voltage curves of cells using G2 electrolyte at 1, 2, and 3 C. In-situ XRD patterns of cells using G2 (f) and EC/DEC (g) electrolytes. (h) Na^- TOF-SIMS mapping of HC anodes before Na plating (left) and after Na plating (right) using G2 and EC/DEC electrolytes.

that engineering a NaF-rich SEI on the HC anode could enable reversible and stable Na plating, paving the way for fast-charging and high-energy-density SIBs. However, a detailed mechanistic understanding of electrolyte-dependent Na plating on HC remains limited, posing a critical gap for rational electrolyte design.

Herein, we investigate the Na plating behavior of HC in practical pouch-type full cells and establish electrolyte design principles, emphasizing that Na plating/stripping reversibility must be considered alongside Na^+ insertion/extraction. Even with an optimized N/P (negative capacity/positive capacity) ratio, Na deposition persists under fast charging, extended cycling and low-temperature operation, underscoring its intrinsic nature. Comparative analysis reveals that, relative to conventional ester-based electrolyte (EC/DEC), ether-based electrolyte (G2) significantly enhances Na plating/stripping reversibility. This improvement is attributed to the lower Na^+ desolvation energy, faster interfacial kinetics, and the formation of a uniform, inorganic-rich SEI. These advantages not only alleviate N/P ratio constraints but also enable higher energy density designs. Thus, optimal electrolytes for HC-based SIBs must concurrently improve Na^+ intercalation kinetics and regulate the Na plating/stripping behavior. Insights from sodium−metal batteries, particularly those related to deposition morphology control and SEI stabilization, can be readily translated to HC-based systems to enhance interfacial regulation.[23] Furthermore, this finding suggests the potential to move beyond the reliance on ester-based electrolyte in low-voltage SIBs (operating <3.5 V vs Na/Na^+), thereby unlocking broader prospects for ether-based systems. Overall, this study offers critical mechanistic insights and guidance for electrolyte engineering for HC anodes in high-performance SIBs.

DETRIMENTAL EFFECTS OF IRREVERSIBLE NA PLATING

HC anodes are among the most commercially viable candidates for SIBs due to their unique advantages. Nevertheless, their low-voltage plateau region lies dangerously close to the sodium deposition potential, making them highly susceptible to irreversible Na plating under actual operating conditions.[9] Specifically, Na plating behavior is observed on the HC anode under a relatively large charging rate of 2 C with an electrolyte of 1 M $NaPF_6$ in the ethylene carbonate and diethyl carbonate (EC/DEC), where the mismatch between ion transport kinetics and storage capacity induces Na deposition (Figure 1a). This is directly verified by precise potential tracking in a three-electrode configuration using a Na metal reference. Irreversible Na plating also intensifies during extended cycling, primarily due to the continuous thickening of the SEI, which hinders ion diffusion at the electrode−electrolyte interface (Figure 1b). Moreover, low-temperature operation exacerbates this issue in which the sharp rise in cell impedance under cold conditions increases the ionic diffusion barrier, thereby triggering Na plating (Figure 1c).

https://doi.org/10.1021/acsenergylett.5c04116
ACS Energy Lett. XXXX, XXX, XXX−XXX

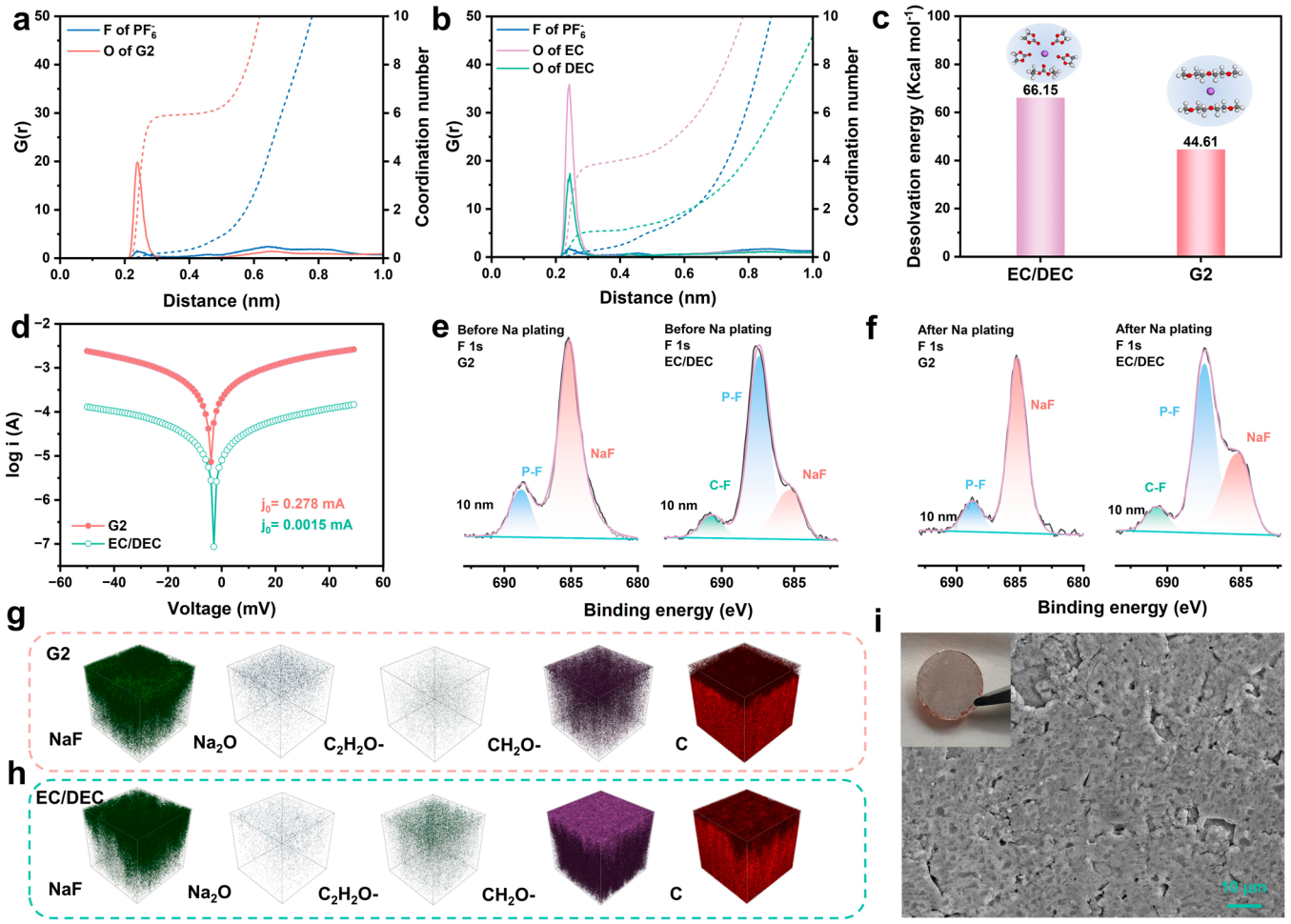

Figure 3. Radial distribution function (RDF) and coordination number analyses obtained from MD simulations for G2 (a) and EC/DEC (b) electrolytes. (c) Calculated dissociation energies for EC/DEC and G2 electrolytes. (d) Tafel plots of the Na electrode using G2 and EC/DEC electrolytes. The in-depth XPS spectra of F 1s before (e) and after Na plating (f) using G2 and EC/DEC electrolytes. TOF-SIMS 3D reconstruction models of SEI components formed in G2 (g) and EC/DEC electrolytes (h) before Na plating. (i) SEM image of Na plating on Cu current collector in G2 electrolyte.

The consequences of irreversible Na deposition are severe, which not only cause capacity decay but also compromise safety performance by inducing gas evolution, heat accumulation, and heightened hazard potential. As shown in Figure 1d, cells subjected to irreversible Na plating exhibit pronounced capacity fading and significant swelling, with cell thickness increasing by 31 μm. Gas analysis from the corresponding pouch cell with Na plating (Figure 1f) reveals the evolution of flammable gases such as H_2, C_2H_4, and CO, which pose major safety hazards. Furthermore, electrode titration experiments show that electrode after cycling releases substantially more H_2 upon reaction with H_2O compared with a normal electrode, confirming the accumulation of irreversibly deposited Na ("dead Na") on the surface (Figure 1g). Beyond gas evolution, the heat generation and safety characteristics of the cell were further investigated. Forward-looking infrared camera (FLIR) (Figure 1h) reveals significant heat accumulation during the charging process in the cell occurring irreversible Na plating, with the overall temperature considerably higher than that of normal cell. Nail penetration testing further emphasizes this risk. Although catastrophic thermal runaway did not occur due to the limited cell capacity, the cell with irreversible Na plating experienced a rapid temperature rise, averaging approximately 2.5 °C higher than that of a normal cell (Figure 1i). Collectively, these results demonstrate that HC-based full cells are prone to irreversible Na plating under fast charging, prolonged cycling, and low-temperature conditions. The associated risks, including gas generation, thermal accumulation, and potential safety failure (Figure 1e) critically limit their practical application and underscore the urgent need to improve the reversibility of Na plating for safe and scalable SIB deployment.

EVALUATION OF NA PLATING REVERSIBILITY

Elucidating the mechanistic basis of electrolyte-controlled Na plating on HC anodes is crucial for the rational electrolyte design. Generally, an ether-based electrolyte exhibits markedly better compatibility in Na metal systems compared to an ester-based electrolyte, enabling higher Coulombic efficiency (CE). To quantitatively assess the reversibility of Na plating/stripping on HC anodes, constant sodiation cycling (CSC) tests were conducted using commercial HC as the model anode (see Figure S1 for basic material characterizations). The CSC protocol involves a full constant-capacity sodiation step followed by desodiation to 2 V (vs Na/Na^+). As shown in Figure 2a,b, HC in G2 electrolyte delivers nearly identical desodiation capacities following constant-capacity sodiation,

https://doi.org/10.1021/acsenergylett.5c04116
ACS Energy Lett. XXXX, XXX, XXX−XXX

revealing highly reversible Na plating/stripping. In contrast, HC in the EC/DEC electrolyte exhibits incomplete Na recovery, reflecting substantially lower reversibility. Increasing the areal capacity to 1.5 mAh cm^{-2} (with Na plating accounting for 37% of total capacity) severely deteriorates reversibility in EC/DEC electrolyte, resulting in initial Coulombic efficiency (ICE) of only 76.74% and a sudden drop in CE after 40 cycles at 1 C (Figure 2c,d). Further increasing the areal capacity to 2.5 mAh cm^{-2} leads to even greater cycling instability (Figure S2a). Furthermore, to demonstrate the generality of electrolyte selection, CSC tests are also performed with two additional ester-based electrolytes, namely, EC/DEC-5% FEC and 1 M $NaClO_4$ in propylene carbonate containing 5% FEC (Figure S3), displaying poor Na plating reversibility. In contrast, G2 electrolyte exhibits excellent cycling stability across various rates at areal capacity of 1.5 mAh cm^{-2}, with ICE of 94.73%, 94.76%, and 93% at 1, 2, and 3 C, respectively, and maintains an average Coulombic efficiency of 99.9% during extended cycling (Figure 2c,e). Notably, the G2 electrolyte retains stable cycling up to an areal capacity of 2.5 mAh cm^{-2} (Figure S2c, d) and still supports reversible Na plating/stripping at a higher areal capacity of 3.1 mAh cm^{-2} (corresponding to 65% Na plating contribution) (Figure S2b), underscoring its exceptional compatibility with HC anodes.

In situ X-ray diffraction (XRD) measurement was employed to further probe the difference in Na plating reversibility between two electrolytes. As shown in Figure 2f, during CSC test of HC in G2 electrolyte, a diffraction peak at 29.4° corresponding to metallic Na[24,25] emerges during sodiation and disappears after desodiation, confirming the highly reversible Na plating/stripping. Conversely, in EC/DEC electrolyte, the metallic Na peak persists throughout desodiation, signifying incomplete Na removal and limited reversibility (Figure 2g, Figure S4). Ex-situ scanning electron microscopy (SEM) observations corroborate this result. In G2 electrolyte, Na deposition initially nucleate along the surface of large HC particles and gradually evolves into a smooth and uniform morphology that can be fully stripped without leaving behind "dead Na" (Figure S5a1−a5). Optical microscopy further confirms the absence of residual metallic Na even after 100 cycles (Figure S6). By comparison, Na deposition in EC/DEC electrolyte produces a bubble-like morphology and these Na bubbles cannot be fully removed during desodiation (Figure S5b1−b5), gradually forming electrically isolated "dead Na", as further confirmed by optical images (Figure S5c1−c5). To gain further insight into Na distribution, time-of-flight secondary ion mass spectrometry (TOF-SIMS) mapping was performed. As shown in Figure 2h, Na^- mapping of HC electrode reveals a uniform spatial distribution in G2 electrolyte, whereas it exhibits pronounced local Na enrichment and poor uniformity in EC/DEC electrolyte. This is further corroborated by C^- mapping, which reveals that the HC surface in the G2 electrolyte remains essentially unchanged after Na plating. In contrast, the C distribution changes significantly before and after Na plating in the EC/DEC electrolyte, confirming the surface reconstruction (Figure S7). Collectively, this finding demonstrates that the reversibility of Na plating/stripping is intimately governed by deposition morphology, with G2 electrolyte enabling smooth, uniform, and reversible Na deposition, in sharp contrast to the unstable and irreversible behavior observed in EC/DEC electrolyte.

EFFECT OF NA PLATING BEHAVIOR

To gain deeper insight into intrinsic structural differences, molecular dynamics (MD) simulations were conducted to elucidate the solvation structures of the two electrolytes. The radial distribution function (RDF) shows that Na^+ is primarily coordinated by G2 molecules in the first solvation shell with a coordination number of two in the G2 electrolyte (Figure 3a). In contrast, a more pronounced EC peak appears in the first solvation shell, where Na^+ forms five-coordinate complexes with EC and DEC molecules in the EC/DEC electrolyte (Figure 3b). This is consistent with the molecular electrostatic potential (MESP) of the solvents, reflecting the higher polarity and stronger binding of the EC molecules (Figure S8). Desolvation energy calculations further reveal that G2 possesses a lower desolvation energy (Figure 3c), reflecting weaker Na^+-solvent interactions. Such a high-energy Na^+ state facilitates reduction and accelerates interfacial charge-transfer kinetics.[26] Furthermore, analysis of temperature-dependent electrochemical impedance spectroscopy (EIS) spectra (Figure S9) reveals that the charge-transfer energy barrier in the EC/DEC electrolyte is higher than that in the G2 electrolyte. Tafel measurement corroborates this, showing a higher exchange current density in the G2 electrolyte, indicative of faster interfacial reactions (Figure 3d). The enhanced interfacial kinetics help mitigate Na^+ concentration gradients and suppress dendrite formation.[27] Moreover, the G2 electrolyte exhibits a lower polarization voltage and interfacial impedance, further confirming its superior interfacial kinetics (Figure S10).

The SEI composition of HC before and after Na plating in the two electrolytes was then analyzed using XPS and TOF-SIMS. Before Na plating, the C 1s and O 1s spectra exhibit stronger C−O and C = O signals in EC/DEC electrolyte compared with G2 electrolyte, implying the formation of more organic-rich SEI (Figure S11a−d).[19] In-depth XPS analysis reveals SEI in EC/DEC electrolyte remains organic-rich even in deeper layer (Figure S12), consistent with 3D TOF-SIMS reconstruction models showing dominant CH_2O^- and $C_2H_2O^-$ signals (Figure 3g,h).[28,29] Both surface (Figure S11e,f) and in-depth (Figure 3e) F 1s spectra show stronger NaF peaks in the G2 electrolyte, demonstrating inorganic-rich SEI components, further supported by 3D TOF-SIMS mapping of NaF and Na_2O (Figure 3g,h, Figure S13a). The quantitative XPS analysis further demonstrates that SEI formed in the G2 electrolyte contains a higher fraction of inorganic components than that formed in the EC/DEC electrolyte (Figures S14 and S15). Atomic force microscopy (AFM) analysis of the SEI mechanical property reveals that the SEI formed in the G2 electrolyte possesses a significantly higher elastic modulus than that generated in the EC/DEC electrolyte, corroborating the formation of an inorganic-rich SEI in the G2 electrolyte (Figure S16). Additionally, the higher C signal detected in G2 electrolyte relative to EC/DEC electrolyte (Figure S13b) reflects the formation of a thinner SEI, likely resulted from reduced solvent decomposition and a greater contribution from inorganic species.[26] Overall, before Na plating, G2 electrolyte forms a thinner, inorganic-rich SEI, whereas EC/DEC electrolyte produces a thicker, organic-rich SEI. It is widely recognized that NaF-rich SEI components facilitate high ionic conductivity, suppress dendrite growth, and enhance structural stability, thereby preventing SEI collapse.[20,21,30,31]

https://doi.org/10.1021/acsenergylett.5c04116
ACS Energy Lett. XXXX, XXX, XXX−XXX

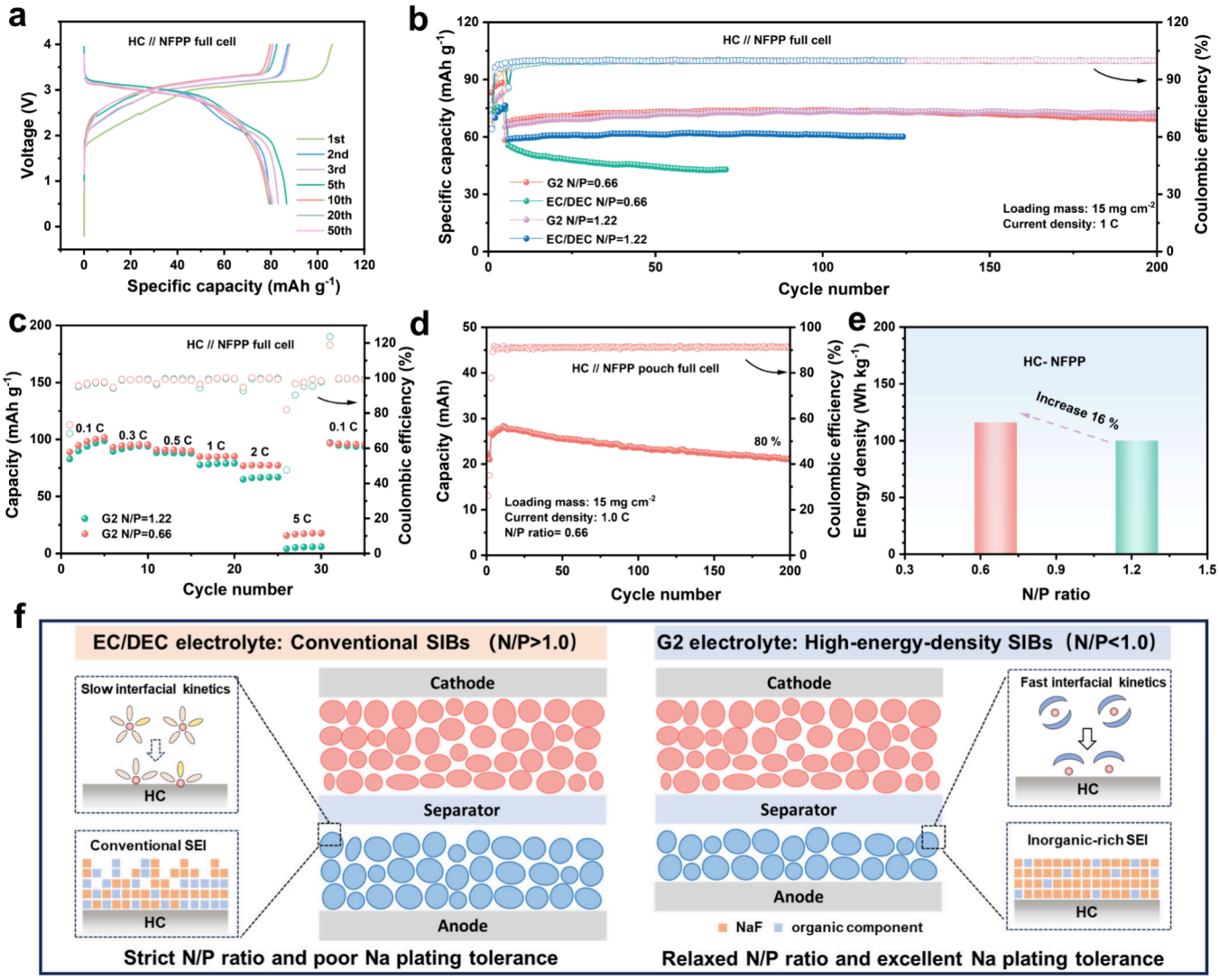

Figure 4. (a) Capacity-voltage profiles of HC//NFPP full cell with a N/P ratio of 0.66 in G2 electrolyte. (b) Cycling performance of HC//NFPP full cell at 1 C. (c) Rate performance of HC//NFPP full cell with N/P ratio of 1.22 and 0.66 in G2 electrolyte. (d) Cycling performance of HC//NFPP pouch full cell with N/P ratio of 0.66 at 1 C using G2 electrolyte. (e) Energy density comparison of SIBs pouch cell with different N/P ratios. (f) Schematic illustration of SEI structure, interfacial kinetics on HC anode, and their implications for low N/P ratio full cells.

After Na plating, in-depth XPS (Figure 3f and Figure S17) and 3D TOF-SIMS profiling (Figure S18) reveal an increased presence of inorganic components in SEI of the EC/DEC electrolyte, indicative of destabilization and reconstruction of SEI induced by irregular Na plating. In contrast, the SEI formed in G2 electrolyte shows only minor composition changes, reflecting greater structural stability. To further investigate the morphology of deposited Na, deposition experiment was conducted on Cu current collector. Figure 3i shows that Na deposited in the G2 electrolyte results in a uniform, dense, and smooth morphology, dominated by large particles with almost no cracks. Conversely, Na deposited in the EC/DEC electrolyte exhibits a loosely packed, irregular structure of small particles, which promotes increased parasitic reactions with the electrolyte (Figure S19). Moreover, when HC electrode precycled in G2 electrolyte was transferred to EC/DEC electrolyte, CSC tests still showed rapid performance decay (Figure S20), demonstrating that the reversibility of Na plating is not solely determined by the SEI composition, but also critically depends on interfacial kinetics and the optimized solvation structure of the electrolyte. Overall, the optimized solvation structure combined with enhanced interfacial kinetics in G2 electrolyte promotes the generation of stable SEI species, offering a clear mechanistic explanation for its highly reversible Na plating behavior.

PROOF-OF-CONCEPT IN FULL CELL

The high reversibility of Na plating in the G2 electrolyte was further confirmed in a full cell with HC as the anode and $Na_4Fe_3(PO_4)_2P_2O_7$ (NFPP) as the cathode. To deliberately induce Na plating on the anode, the N/P ratio was set to 0.66. Voltage-capacity profiles and cycling test (Figure 4a,b) show that HC//NFPP full cell in G2 electrolyte exhibits stable cycling at 1 C comparable to cell with conventional N/P ratio, and sustains 86.6% capacity retention over 300 cycles at 0.5 C, demonstrating highly reversible Na plating and long-term stability (Figure S21). Optical and SEM images (Figure S22) reveal that the HC anode remains smooth and free of noticeable dead sodium after 100 cycles, consistent with excellent electrochemical performance. In contrast, HC// NFPP full cell in EC/DEC electrolyte show significantly lower

https://doi.org/10.1021/acsenergylett.5c04116
ACS Energy Lett. XXXX, XXX, XXX−XXX

capacity and poorer cycling stability, with capacity retention falling to 76.6% after 70 cycles, likely due to continuous SEI rupture and reconstruction caused by repeated Na deposition. Notably, the HC//NFPP full cell in the G2 electrolyte maintains a higher reversible capacity and stable CE across a wide rate range of 0.1−5 C, demonstrating excellent Na plating reversibility even at 5 C (Figure 4c). HC//NVP ($Na_3V_2(PO_4)_3$) full cell with a N/P ratio of 0.66 was also assembled in G2 electrolyte, achieving an ICE of 70.5% (Figure S23). To assess practical applicability, pouch full cell HC//NFPP with cathode mass loading of 15 mg cm^{-2} were assembled, demonstrating stable cycling for 200 cycles at 1 C with a capacity retention of 80% (Figure 4d). Inspiringly, compared with the soft-pack full cell with normal N/P ratio, lowering the N/P ratio to 0.66 allows the additional capacity from deposited Na to enhance energy density by 16% (Figure 4e). Therefore, achieving stable cycling at low N/P ratio not only improves overall energy density but also substantially reduces material costs. We further performed differential scanning calorimetry (DSC) to quantitatively assess the heat-generation behavior of the sodiated HC-electrolyte mixtures and charged NFPP-electrolyte mixtures (Figures S24 and S25).The result shows that the total heat release of sodiated HC-electrolyte mixtures is nearly identical in the two electrolytes, while the NFPP cathode exhibits slightly lower heat generation in the G2 electrolyte compared with the EC/DEC electrolyte. Therefore, using the G2 electrolyte in low-voltage systems does not introduce additional heat-generation risks relative to EC/DEC electrolyte.

Figure 4f highlights the fundamental differences in the SEI structure and full-cell application between the two electrolytes. The lower desolvation energy of G2 electrolyte facilitates the formation of a smooth, dense, and inorganic-rich SEI on the HC anode, which is highly ionically conductive and enables compact, reversible Na plating while preserving structural integrity during repeated plating/stripping. The combination of such robust SEI and fast interfacial kinetics allows full cells to operate stably at low N/P ratio, thereby achieving higher energy density and reducing material cost. In contrast, HC in EC/DEC electrolyte forms a thicker, organic-rich SEI that hinders ion diffusion, induces nonuniform nucleation sites, and facilitates Na dendrite growth. Continuous Na plating/stripping under these conditions result in repeated SEI rupture and reconstruction, leading to gradual performance decay. Consequently, full-cell design in EC/DEC electrolyte must carefully control the N/P ratio to prevent Na deposition and maintain stable cycling performance. This finding suggests that electrolyte design for HC-based system requires balancing stable Na insertion/extraction with controlled Na plating/stripping, which is critical for full-cell performance, allowing relaxed N/P ratios and enhanced overall energy density.

In conclusion, this work establishes that Na plating in HC anodes is an intrinsic and unavoidable phenomenon under practical full-cell operating conditions, including fast charging, prolonged cycling, and low-temperature operation. Systematic comparison between ester-based (EC/DEC) and ether-based (G2) electrolytes demonstrates that G2 electrolyte enables highly reversible Na plating/stripping due to lower desolvation energy, faster interfacial kinetics, and uniform inorganic-rich SEI. These insights reveal that electrolyte design for HC-based systems must move beyond merely facilitating Na^+ insertion/extraction to simultaneously ensuring stable Na plating/stripping behavior. Such a dual design principle not only alleviates N/P ratio constraints but also provides a pathway toward safer, higher-energy-density SIBs. Ultimately, the mechanistic understanding developed here offers valuable guidance for advancing electrolyte engineering strategies and accelerating the practical deployment of HC-based SIBs.

■ ASSOCIATED CONTENT

Supporting Information

The Supporting Information is available free of charge at https://pubs.acs.org/doi/10.1021/acsenergylett.5c04116.

Experiment methods, characterizations, and additional electrochemical data (PDF)

■ AUTHOR INFORMATION

Corresponding Authors

Yang Yang − *College of Chemistry and Chemical Engineering and State-Province Joint Engineering Laboratory of Power Source Technology for New Energy Vehicle, State Key Laboratory of Physical Chemistry of Solid Surfaces, Engineering Research Center of Electrochemical Technology, Ministry of Education, Collaborative Innovation Center of Chemistry for Energy Materials, Xiamen University, Xiamen 361005, P. R. China*; orcid.org/0000-0003-4215-5767; Email: yangyang419@xmu.edu.cn

Jinbao Zhao − *College of Chemistry and Chemical Engineering and State-Province Joint Engineering Laboratory of Power Source Technology for New Energy Vehicle, State Key Laboratory of Physical Chemistry of Solid Surfaces, Engineering Research Center of Electrochemical Technology, Ministry of Education, Collaborative Innovation Center of Chemistry for Energy Materials, Xiamen University, Xiamen 361005, P. R. China*; orcid.org/0000-0002-2753-7508; Email: jbzhao@xmu.edu.cn

Authors

Yuejing Zeng − *College of Chemistry and Chemical Engineering and State-Province Joint Engineering Laboratory of Power Source Technology for New Energy Vehicle, State Key Laboratory of Physical Chemistry of Solid Surfaces, Engineering Research Center of Electrochemical Technology, Ministry of Education, Collaborative Innovation Center of Chemistry for Energy Materials, Xiamen University, Xiamen 361005, P. R. China*

Wei Li − *College of Chemistry and Chemical Engineering and State-Province Joint Engineering Laboratory of Power Source Technology for New Energy Vehicle, State Key Laboratory of Physical Chemistry of Solid Surfaces, Engineering Research Center of Electrochemical Technology, Ministry of Education, Collaborative Innovation Center of Chemistry for Energy Materials, Xiamen University, Xiamen 361005, P. R. China*

Yuan Qin − *College of Chemistry and Chemical Engineering and State-Province Joint Engineering Laboratory of Power Source Technology for New Energy Vehicle, State Key Laboratory of Physical Chemistry of Solid Surfaces, Engineering Research Center of Electrochemical Technology, Ministry of Education, Collaborative Innovation Center of Chemistry for Energy Materials, Xiamen University, Xiamen 361005, P. R. China*

Complete contact information is available at: https://pubs.acs.org/10.1021/acsenergylett.5c04116

Author Contributions

#Y.Z. and W.L. contributed equally to this work.

Notes

The authors declare no competing financial interest.

■ ACKNOWLEDGMENTS

We gratefully acknowledge the financial support of National Key Research and Development Program of China (2021YFB2400300), National Natural Science Foundation of China (22109030, 22021001), The Key Research and Development Program of Yunnan Province (202103AA080019), and the Fundamental Research Funds for the Central Universities (20720220073). We also acknowledge the help of the Tan Kah Kee Innovation Laboratory on the scientific tests. The numerical calculations in this paper have been done at the Hefei advanced computing center. The authors would particularly like to acknowledge Prof. Jiawei Yan and groupmate Xiaoting Yin for their help with the AFM measurement and analysis.

■ REFERENCES

(1) Xue, J.; Zhang, H.; Chen, J.; Fang, K.; Chen, Y.; Zou, Y.; Hong, Y.; Qiao, Y.; Sun, S.-G. Unlocking the Na-Storage Behavior in Hard Carbon Anode by Mass Spectrometry. *Nano Lett.* **2024**, *24* (32), 9839−9845.

(2) Zeng, Y.; Wang, F.; Cheng, Y.; Chen, M.; Hou, J.; Yang, D.; Zhang, Y.; Yang, W.; Liu, G.; Zhang, Y.; Zhu, Z.; Li, X.; Yang, Y.; Zhao, J. Identifying the Importance of Functionalization Evolution during Pre-Oxidation Treatment in Producing Economical Asphalt-Derived Hard Carbon for Na-Ion Batteries. *Energy Storage Mater.* **2024**, *73*, No. 103808.

(3) Li, W.; Xie, H.; Lin, S.; Qin, Y.; Zeng, J.; Zhang, P.; Zhao, J. Insights on the Degradation Mechanism of 7 Ah Sodium Ion Batteries at Different Aging Modes. *J. Power Sources* **2025**, *639*, No. 236635.

(4) Yang, H.; Zeng, Y.; Li, W.; Yang, Y.; Zhao, J. The Importance of Fabricating Hard Carbon-Based Full Cells to Overcome Sodium Metal Anode Limitations in Evaluating High-Mass-Loading Cathodes. *ACS Energy Lett.* **2025**, *10* (6), 2868−2876.

(5) Li, Y.; Vasileiadis, A.; Zhou, Q.; Lu, Y.; Meng, Q.; Li, Y.; Ombrini, P.; Zhao, J.; Chen, Z.; Niu, Y.; Qi, X.; Xie, F.; van der Jagt, R.; Ganapathy, S.; Titirici, M.-M.; Li, H.; Chen, L.; Wagemaker, M.; Hu, Y.-S. Origin of Fast Charging in Hard Carbon Anodes. *Nat. Energy* **2024**, *9* (2), 134−142.

(6) Zeng, Y.; Yang, J.; Yang, H.; Yang, Y.; Zhao, J. Bridging Microstructure and Sodium-Ion Storage Mechanism in Hard Carbon for Sodium Ion Batteries. *ACS Energy Lett.* **2024**, *9* (3), 1184−1191.

(7) Li, Z.; Ma, L.; Surta, T. W.; Bommier, C.; Jian, Z.; Xing, Z.; Stickle, W. F.; Dolgos, M.; Amine, K.; Lu, J.; Wu, T.; Ji, X. High Capacity of Hard Carbon Anode in Na-Ion Batteries Unlocked by POx Doping. *ACS Energy Lett.* **2016**, *1* (2), 395−401.

(8) Zheng, Z.; Hu, S.; Yin, W.; Peng, J.; Wang, R.; Jin, J.; He, B.; Gong, Y.; Wang, H.; Fan, H. J. CO_2 -Etching Creates Abundant Closed Pores in Hard Carbon for High-Plateau-Capacity Sodium Storage. *Adv. Energy Mater.* **2024**, *14* (3), No. 2303064.

(9) Dai, S.; Tu, Y.; Yan, L.; Li, Y.; Ma, M.; Huang, R.; Yao, X.; Pan, H. Observation and Suppression of Metallic and Metallic-like Plating on Hard Carbon for High-Performance Sodium-Ion Batteries. *Mater. Today Energy* **2024**, *44*, No. 101605.

(10) Bommier, C.; Surta, T. W.; Dolgos, M.; Ji, X. New Mechanistic Insights on Na-Ion Storage in Nongraphitizable Carbon. *Nano Lett.* **2015**, *15* (9), 5888−5892.

(11) Chen, X.; Liu, C.; Fang, Y.; Ai, X.; Zhong, F.; Yang, H.; Cao, Y. Understanding of the Sodium Storage Mechanism in Hard Carbon Anodes. *Carbon Energy* **2022**, *4* (6), 1133−1150.

(12) Masias, A.; Marcicki, J.; Paxton, W. A. Opportunities and Challenges of Lithium Ion Batteries in Automotive Applications. *ACS Energy Lett.* **2021**, *6* (2), 621−630.

(13) Tang, C.; Fan, X.; Shi, J.; Zhong, J.; Wang, Q.; Guo, X. Quantitative Decoupling of Electrode Expansion, Electrolyte Depletion, and Dead Sodium in Low-Temperature Storage Cylindrical Sodium-Ion Cell. *Energy Storage Mater.* **2025**, *81*, No. 104495.

(14) Xu, L.; Xiao, Y.; Yang, Y.; Xu, R.; Yao, Y.; Chen, X.; Li, Z.; Yan, C.; Huang, J. In Situ Li-Plating Diagnosis for Fast-Charging Li-Ion Batteries Enabled by Relaxation-Time Detection. *Adv. Mater.* **2023**, *35* (42), No. 2301881.

(15) Yue, X.; Zhang, J.; Dong, Y.; Chen, Y.; Shi, Z.; Xu, X.; Li, X.; Liang, Z. Reversible Li Plating on Graphite Anodes through Electrolyte Engineering for Fast-Charging Batteries. *Angew. Chem., Int. Ed.* **2023**, *62* (19), No. e202302285.

(16) Deng, W.; Yang, H.; Huo, H.; Yu, Y. Recent Advances, Key Strategies, and Challenges in Fast-Charging Hard Carbon Anodes for Sodium-Ion Batteries. *Adv. Funct. Mater.* **2025**, *35* (37), No. 2504168.

(17) Li, W.; Lin, S.; Xie, H.; Qin, Y.; Wu, Q.; Zeng, J.; Zhang, P.; Zhao, J. Uncovering Sodiated HC Dominated Thermal Runaway Mechanism of NFPP/HC Pouch Battery. *Appl. Energy* **2025**, *391*, No. 125936.

(18) Liu, X.; Zhao, J.; Dong, H.; Zhang, L.; Zhang, H.; Gao, Y.; Zhou, X.; Zhang, L.; Li, L.; Liu, Y.; Chou, S.; Lai, W.; Zhang, C.; Chou, S. Sodium Difluoro(Oxalato)Borate Additive-Induced Robust SEI and CEI Layers Enable Dendrite-Free and Long-Cycling Sodium-Ion Batteries. *Adv. Funct. Mater.* **2024**, *34* (37), No. 2402310.

(19) Dong, Y.; Chen, Y.; Yue, X.; Liang, Z. Unveiling the Adsorption Tendency of Film-Forming Additives to Enable Fast-Charging Hard Carbon Anodes with Regulated Li Plating. *Energy Environ. Sci.* **2024**, *17* (7), 2500−2511.

(20) Li, K.; Zhang, J.; Lin, D.; Wang, D.-W.; Li, B.; Lv, W.; Sun, S.; He, Y.-B.; Kang, F.; Yang, Q.-H.; Zhou, L.; Zhang, T.-Y. Evolution of the Electrochemical Interface in Sodium Ion Batteries with Ether Electrolytes. *Nat. Commun.* **2019**, *10*, 725.

(21) Zhang, J.; Wang, D.-W.; Lv, W.; Zhang, S.; Liang, Q.; Zheng, D.; Kang, F.; Yang, Q.-H. Achieving Superb Sodium Storage Performance on Carbon Anodes through an Ether-Derived Solid Electrolyte Interphase. *Energy Environ. Sci.* **2017**, *10* (1), 370−376.

(22) Dong, Y.; Zeng, Q.; Ding, L.; Qi, A.; Shen, Y.; Fang, M.; Shi, Z.; Chen, Y.; Song, H.; Wang, R.; Yue, X.; Liang, Z. Modulating Na Plating Morphology via Interfacial Design to Achieve Energy-Dense and Fast-Charging Sodium-Ion Batteries. *Nano Energy* **2025**, *136*, No. 110777.

(23) Wan, S.; Song, K.; Chen, J.; Zhao, S.; Ma, W.; Chen, W.; Chen, S. Reductive Competition Effect-Derived Solid Electrolyte Interphase with Evenly Scattered Inorganics Enabling Ultrahigh Rate and Long-Life Span Sodium Metal Batteries. *J. Am. Chem. Soc.* **2023**, *145* (39), 21661−21671.

(24) Liu, X.; Zhang, M.; Wang, X.; Peng, Y.; Liu, Y.; Ullah, S.; Duan, Z.; Gao, W.; Song, B.; Wei, M.; He, J.; Li, Z.; Wu, Y. Evidence of Quasi-Na Metallic Clusters in Sodium Ion Batteries through In Situ X-Ray Diffraction. *Adv. Mater.* **2025**, *37* (1), No. 2410673.

(25) Wang, C.; Wang, K.; Ni, H.; Du, C.; Yin, X.; Fan, J.; Yuan, R.; Tang, Y.; Yan, J.; Zheng, M.; Dong, Q. Reinvented Sodium Anode by Creating a Metal-Bulk Storage Matrix with an Expanded 3D Plating/Stripping Mechanism. *Sci. Adv.* **2025**, *11* (27), eadw5701.

(26) Xu, X.; Yue, X.; Chen, Y.; Liang, Z. Li Plating Regulation on Fast-Charging Graphite Anodes by a Triglyme-$LiNO_3$ Synergistic Electrolyte Additive. *Angew. Chem., Int. Ed.* **2023**, *62* (34), No. e202306963.

(27) Liu, J.; Hua, H.; Lin, J.; Deng, Y.; Pei, N.; Zhang, P.; Dong, J.-C.; Li, J.-F.; Zhao, J. Optimizing Interface Concentration and Electric Fields for Enhanced Lithium Deposition Behavior in Lithium Metal Anodes. *Energy Environ. Sci.* **2024**, *17* (16), 5993−6002.

(28) Zhong, S.; Yu, Y.; Yang, Y.; Yao, Y.; Wang, L.; He, S.; Yang, Y.; Liu, L.; Sun, W.; Feng, Y.; Pan, H.; Rui, X.; Yu, Y. Molecular Engineering on Solvation Structure of Carbonate Electrolyte toward

https://doi.org/10.1021/acsenergylett.5c04116
ACS Energy Lett. XXXX, XXX, XXX−XXX

Durable Sodium Metal Battery at − 40 °C. *Angew. Chem., Int. Ed.* **2023**, *62* (18), No. e202301169.
(29) Jin, Y.; Le, P. M. L.; Gao, P.; Xu, Y.; Xiao, B.; Engelhard, M. H.; Cao, X.; Vo, T. D.; Hu, J.; Zhong, L.; Matthews, B. E.; Yi, R.; Wang, C.; Li, X.; Liu, J.; Zhang, J.-G. Low-Solvation Electrolytes for High-Voltage Sodium-Ion Batteries. *Nat. Energy* **2022**, *7* (8), 718−725.
(30) Han, M.; Zhu, C.; Ma, T.; Pan, Z.; Tao, Z.; Chen, J. In Situ Atomic Force Microscopy Study of Nano−Micro Sodium Deposition in Ester-Based Electrolytes. *Chem. Commun.* **2018**, *54* (19), 2381−2384.
(31) Luo, J.; Yang, K.; Gai, J.; Zhang, X.; Peng, C.; Qin, C.; Ding, Y.; Yuan, Y.; Xie, Z.; Yan, P.; Cao, Y.; Lu, J.; Chen, W. Anion-Tailored EDL Induced Triple-Layer SEI on High-Capacity Anodes Enabling Fast-Charging and Durable Sodium-Storage. *Angew. Chem., Int. Ed.* **2025**, *64* (7), No. e202419490.

https://doi.org/10.1021/acsenergylett.5c04116
ACS Energy Lett. XXXX, XXX, XXX−XXX